Cuadernos de Investigación Geográfica *Geographical Research Letters*	2026	Nº 52 (1)	pp. 153-174	EISSN 1697-9540

http://doi.org/10.18172/cig.7105

FINE-SCALE TOPOCLIMATIC PATTERNS AND THEIR IMPLICATIONS FOR HIGH-ALTITUDE VINEYARDS

GRETHEL GARCÍA BU BUCOGEN[1]*, MAXIMILIANO VIALE[1]
FACUNDO IMPAGLIAZZO[2]

[1] *Instituto Argentino de Nivología, Glaciología y Ciencias Ambientales (IANIGLA), Av. Dr. Ruiz Leal, Mendoza, Argentina.*

[2] *Independent viticulturist (RAQUIS project), RN40, Agrelo, Luján de Cuyo, Mendoza, Argentina.*

ABSTRACT. Understanding the spatial configuration of local climate in mountainous agricultural areas is essential for assessing land suitability and adaptation strategies under global warming. This study aims to quantify fine-scale thermal variability and evaluate its implications for site-specific vineyard management under frost and heat stress conditions. The study area is a high-altitude vineyard (1430–1550 m a.s.l.), known as Monasterio (RAQUIS project), located in Gualtallary, Mendoza (Argentina). Air temperature was recorded every 5–15 minutes using twelve sensors and one automatic weather station over two growing seasons (October–March) and one dormancy period (May–September). Thermal and bioclimatic spatial patterns were examined through point-based measurements and regression-based modelling in SAGA-QGIS. Results show that variations in slope, aspect, and altitude produce strong microclimatic contrasts, delineating two distinct Winkler bioclimatic zones within the vineyard, ranging from cold–moderate to moderate thermal regimes. East-, northeast- and southeast-facing slopes exhibited higher heat accumulation, whereas lower sectors were prone to nocturnal cold-air pooling and frost formation. During the growing season, mean maximum and minimum temperatures differed by up to 3.5°C and 2.5°C, respectively, revealing marked thermal heterogeneity across short distances. This study highlights the role of fine-scale topography in shaping vineyard climates and demonstrates the value of high-resolution climatic monitoring and GIS-based spatial analysis for understanding topoclimatic dynamics in mountainous agricultural environments. These findings contribute to both viticultural adaptation and broader research in physical geography and local climatology.

Patrones topoclimáticos de alta resolución y sus implicaciones para los viñedos de alta altitud

RESUMEN. Comprender la configuración espacial del clima local en áreas agrícolas de montaña es esencial para evaluar la idoneidad del territorio y las estrategias de adaptación frente al calentamiento global. Este estudio tiene como objetivo cuantificar la variabilidad térmica a pequeña escala y evaluar sus implicaciones para la gestión del viñedo de puntos específicos bajo condiciones de heladas y estrés por calor. El área de estudio es un viñedo de altitud (1430–1550 m s. n. m.), conocido como Monasterio (proyecto RAQUIS), ubicado en Gualtallary, Mendoza (Argentina). La temperatura del aire se registró cada 5–15 minutos mediante doce sensores y una estación meteorológica automática durante dos temporadas de crecimiento (octubre–marzo) y un periodo de reposo vegetativo (mayo–septiembre). Los patrones espaciales térmicos y bioclimáticos se analizaron mediante mediciones puntuales y modelización basada en regresiones en SAGA-QGIS. Los resultados muestran que las variaciones en la pendiente, la orientación y la altitud generan fuertes contrastes microclimáticos, delimitando dos zonas bioclimáticas de Winkler dentro del viñedo, que abarcan desde regímenes fríos–moderados hasta moderados. Las laderas orientadas al este, noreste y sureste presentaron mayor acumulación de calor, mientras que los sectores más bajos fueron propensos a la acumulación nocturna de aire frío y a la formación de heladas. Durante la temporada de crecimiento, las temperaturas máximas y mínimas medias difirieron hasta en 3,5°C y 2,5°C, respectivamente, revelando una marcada heterogeneidad térmica en distancias muy cortas. Este estudio pone de relieve el papel de la topografía de pequeña escala en la configuración del clima vitícola y demuestra el valor del monitoreo climático de alta resolución y del análisis espacial basado en SIG para comprender la dinámica topoclimática en entornos agrícolas de montaña. Estos resultados contribuyen tanto a la adaptación vitivinícola como a la investigación más amplia en geografía física y climatología local.

Key words: Topoclimate, thermal variability, terrain analysis, frost risk, precision agriculture.

Palabras clave: Topoclima, variabilidad térmica, análisis del terreno, riesgo de helada, agricultura de precisión.

Received: 9 November 2025

Accepted: 6 March 2026

***Corresponding author:** Instituto Argentino de Nivología, Glaciología y Ciencias Ambientales (IANIGLA), Av. Dr. Ruiz Leal, Mendoza, Argentina. Email: grgarcia@mendoza-conicet.gob.ar

1. Introducción

In high-altitude areas, topographic variability exerts a decisive influence on local climatic conditions, giving rise to heterogeneous microclimates. The topoclimate emerges from the interaction between regional atmospheric circulation and fine-scale landscape attributes such as altitude, slope, aspect, terrain curvature, vegetation cover, and soil properties (Ciazela and Ciazela, 2021). These factors modulate energy and moisture exchanges between the land surface and atmosphere, generating complex thermal patterns with pronounced spatial and temporal variability (Bonnefoy *et al.,* 2012; Jacquet and Morlat, 1997; Orlandini *et al.,* 2006). Such processes operate across a wide range of spatial and temporal scales, from metres to kilometres and from seconds to hours, producing highly variable microclimatic mosaics even within a single plot (Littmann, 2008; Neethling *et al.,* 2019; Yoshino, 1975).

Fine-scale climatic variability is particularly relevant in agricultural systems, where small thermal differences can significantly affect crop performance. In the context of global warming, areas previously considered marginal have gained increasing agricultural relevance. The expansion of high-altitude viticulture has emerged as an adaptive strategy to rising temperatures, given its potential to reduce thermal stress, preserve acidity, extend the growing season, and enhance wine quality (Daskalakis *et al.,* 2025; Lasanta *et al.,* 2022; van Leeuwen *et al.,* 2019). Recent studies report an upward shift in viticultural suitability in several regions (Irimia *et al.,* 2024) and have shown that, in Argentina, Spain and Portugal, higher altitude conditions promote greater aromatic and phenolic complexity in *Vitis vinifera cv.* Cabernet Sauvignon (Deis *et al.,* 2024).

However, establishing vineyards in mountainous or topographically complex environments does not necessarily ensure more favorable conditions. Local factors such as slope, aspect, and solar exposure, together with the frost occurrence can generate adverse or highly variable microclimates. Although altitude increases diurnal thermal amplitude, it may also enhance the risk of late frosts, strong winds, and intense nocturnal cooling.

Despite the growing body of research on high-altitude viticulture, most studies have focused on regional or meso-scale analyses, often overlooking fine-scale thermal variability within individual vineyards. In complex terrains, micro-topographic features can generate strong thermal contrasts over short distances, directly affecting vine performance and management decisions. Moreover, the integration of high-resolution topographic data with dense microclimatic observations remains limited, particularly in the Andean piedmont, where viticulture is rapidly expanding. This limitation constrains the accurate characterization of local climatic conditions and the development of site-specific management strategies.

To address these gaps, this study evaluates the influence of topography on local thermal patterns and their implications for viticulture suitability. The analysis is conducted in a vineyard located between 1430 and 1550 m a.s.l. in Gualtallary (Uco Valley, Mendoza, Argentina), where twelve temperature sensors and an automatic weather station were installed to quantify thermal contrasts associated with complex terrain. The study integrates high-resolution thermal monitoring with GIS-based spatial modelling to: (1) characterize fine-scale thermal variability; (2) delineate thermal zones for differentiated management; and (3) assess implications for site-specific viticulture practices, particularly in relation to frost risk and heat stress. This approach provides a replicable framework for other high-altitude wine-growing regions by combining dense temperature observations, detailed terrain analysis, and regression-based spatial modelling to characterise and map intra-vineyard thermal.

2. Study area

2.1. Regional climate influences

The Raquis Monasterio vineyard is located in the Uco Valley, one of the most important vineyard zones of Argentina, within the central productive oasis of the Mendoza Province (Fig. 1). At the regional scale, the climate of central-western Argentina is strongly influenced by the Andes, which act as an orographic barrier limiting the penetration of Pacific air masses into the continent (Fig. 1a). While central Chile exhibits a Mediterranean climate with winter precipitation, conditions on the eastern side of the Andes (Mendoza and San Juan provinces, Fig. 1a) shift to a semi-arid continental regime. Annual precipitation at Cuyo region is low (~200 mm) and in mainly in concentrated in summer through convective storms (~150 mm), whereas winter precipitations is scarce (~50mm) (Viale and Núñez, 2011; Viale *et al.,* 2019).

The region is characterised by high solar radiation, low atmospheric humidity, and a pronounced diurnal and seasonal thermal amplitude (Servicio Meteorológico Nacional, 2024). Data from the vineyard's meteorological station reflect these regional characteristics (Fig. 2). Incoming solar radiation (Fig. 2a) exceeds 21 MJ m^{-2} day^{-1} during the growing season (October–March), and values above 28 MJ m^{-2} day^{-1} during the veraison and ripeness periods (December–February). Daylight duration varies from approximately 11 hours in winter to nearly 15 hours in summer. Monthly Tmean, Tmin and Tmax range from -4°C, 4°C, and 11°C in July to 13°C, 21°C, and 31°C in January (Fig. 2b). The thermal amplitude remains relatively constant throughout the year, at around 20°C. Regional dryness is further evidenced by low dew point temperature, which range from negative values in winter to approximately 10°C in summer (Fig. 2b). According to Servicio Meteorológico Nacional (2024), these conditions are typical of the Cuyo region and are consistent with the climatology described in the National Climatic Atlas (Servicio Meteorológico Nacional, 2024).

Winds are generally weak throughout the year at the eastern foothills of the Andes (Prohaska, 1976), except during occasional downslope windstorms known as Zonda events. These is a local foehn wind characterised by high temperatures, low humidity, and wind speeds exceeding 40 km h^{-1}, and occur most frequently in winter and spring (Norte, 2015).

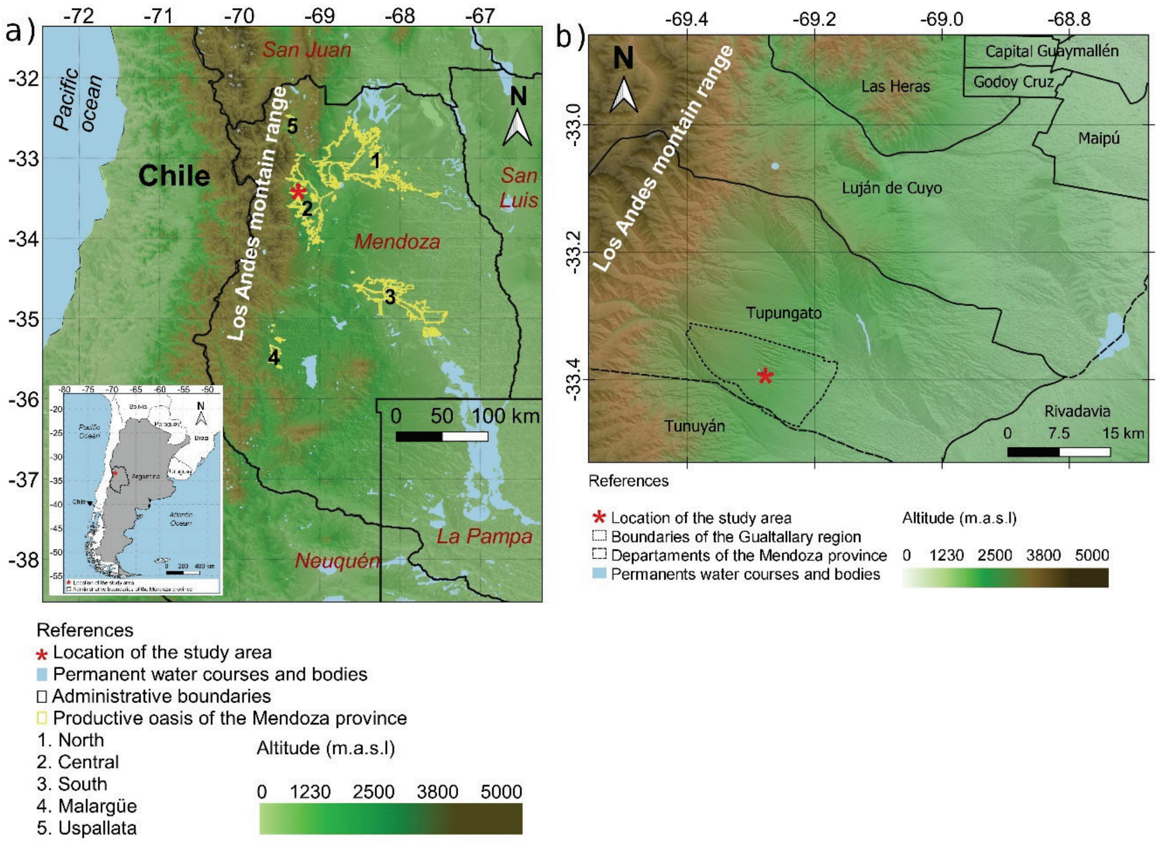

Figure 1. Study area location: (a) regional-scale context and (b) meso-scale detail.

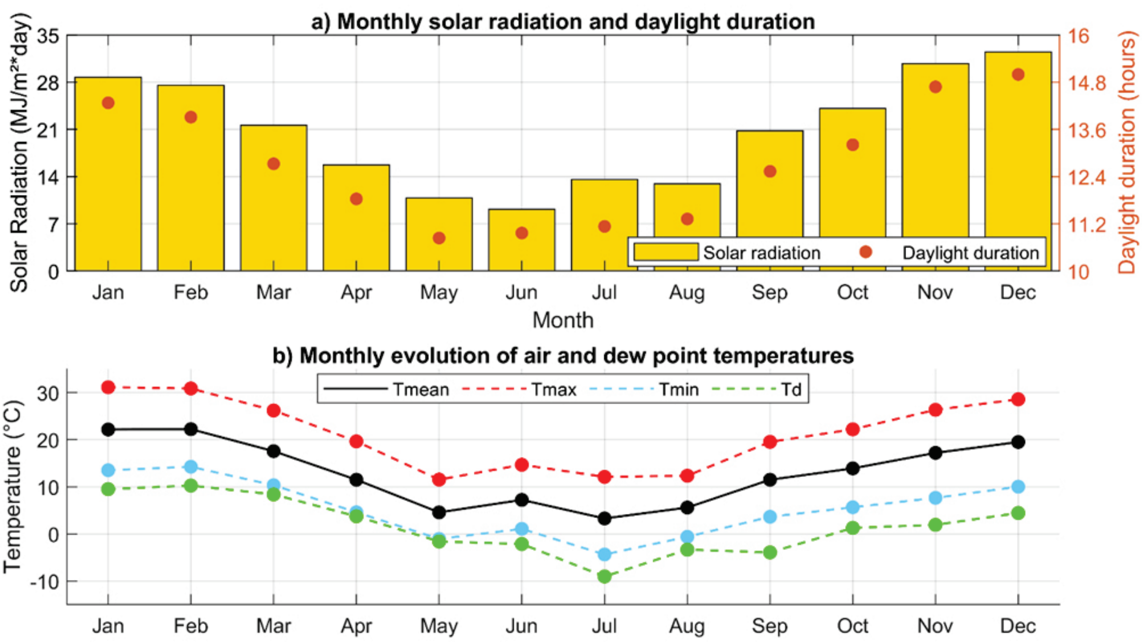

Figure 2. Monthly means of a) incoming solar radiation (MJ m^{-2} per day) and daylight duration (hours), and of b) daily minimum, mean, and maximum temperatures, as well as dewpoint temperatures obtained from two years of records from the weather station in the Raquis Monasterio vineyard.

2.2. Vineyard terrain and its meteorological network

The Raquis Monasterio vineyard extends from 1433 to approximately 1500 m a.s.l. across the piedmont landscape located about 20km east of the Andes foothills. The terrain exhibits marked small-scale variability, including a central hill where sensor 16 is located at the crest (Fig. 3a). The Andes Mountain range Andes reach elevations of approximately 5000 m a.s.l at these latitudes, strongly influencing regional climate and reducing incoming solar radiation near the mountain front.

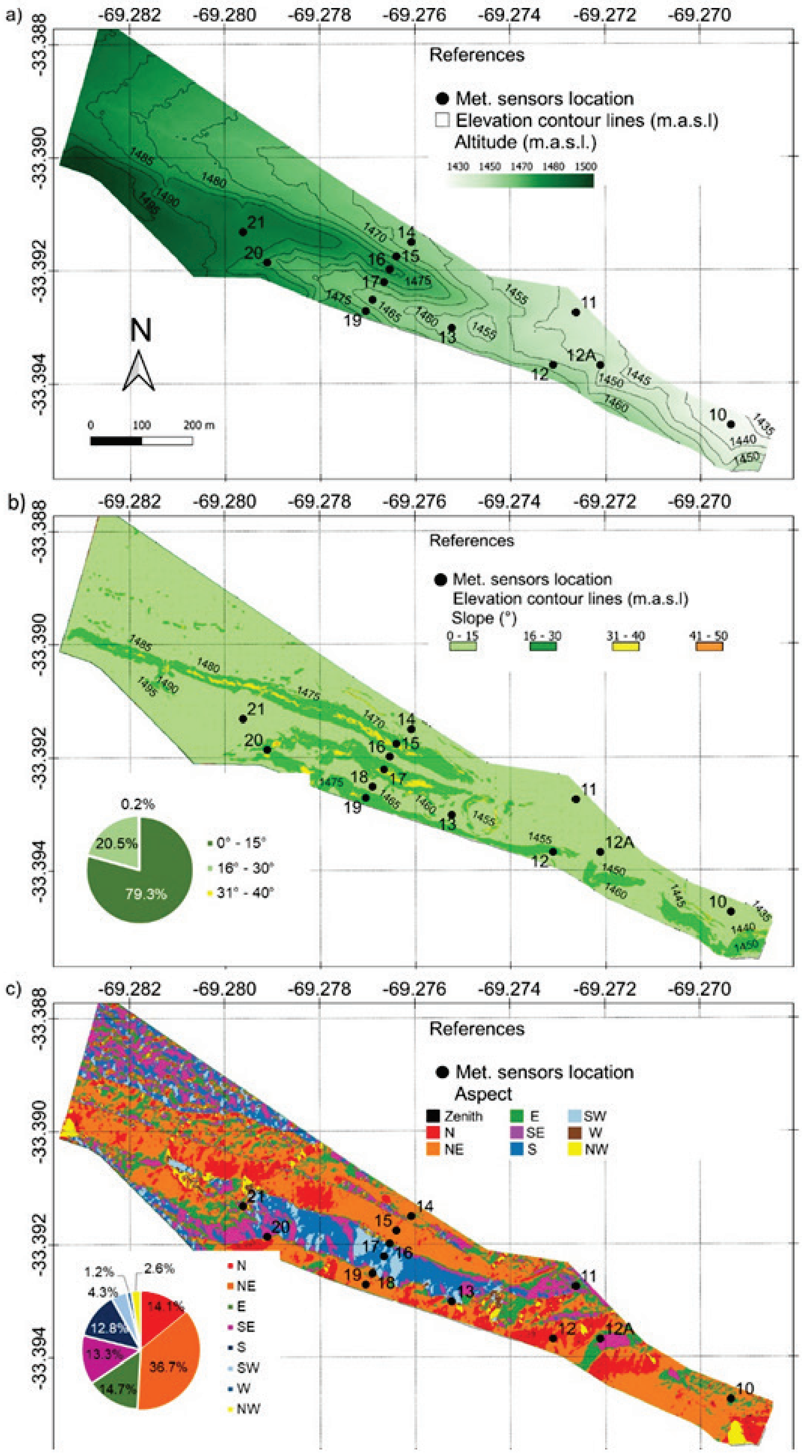

Figure 3. Terrain characteristics of the Raquis Monasterio vineyard: a) altimetry showing the location of temperature sensors, b) slope distribution showing the percentage of area by slope class, c) slope aspect showing the percentage of area by aspect orientation.

The vineyard covers an area of 30.4 hectares, of which 99.8% consists of slopes gentler than 30° (Fig. 3b). The dominant aspect (slope orientation) is northeast (Fig. 3c), except for the southern-central sector, which features slopes facing south and southwest (Fig. 3a and 3b).

The study area was equipped with one μMETOS weather station (id: 12A) and a network of twelve HOBO Pendant MX2201 air temperature sensors (Fig. 4) distributed across the vineyard (Fig. 3 and Table 1). All temperature sensors were installed at 1.5 meters above ground level, following the World Meteorological Organization guidelines (Stel *et al.,* 2019). The HOBO sensors have a manufacturer-specified accuracy of ±0.53°C and a measurement range of −20°C to 70°C, and were housed within passive radiation shields to minimise direct solar exposure. The reference meteorological station (μMETOS 12A) was installed at the same height (1.5 m) and equipped with a ventilated radiation shield, providing high-quality temperature measurements for comparison and correction purposes.

The average altitudinal difference between sensors was 17.1 m, with a maximum difference of 50 m between sensors 10 and 21 (Table 1). The highest sensors (16 and 21) were located on the hill crest and in the western sector of the vineyard (~1480 m a.s.l.). Most sensors were installed on northeast-facing slopes (10, 12, 14, 15, 18, and 19), whereas others were oriented east (12A, 16, and 20), southeast (11, 13, and 21), and southwest (17) (Table 1 and Fig. 3c). The steepest slopes were located near sensors 19, 15, and 17, on both sides of the hill (Fig. 3).

High-frequency temperature data were recorded every 5 minutes by the sensor network and every 15 minutes by 12A weather station, which also measured solar radiation, wind, and humidity. Temperature sensors recorded data from October 30, 2022, whereas 12A weather station began measurements on September 19, 2023. In the Southern Hemisphere, the grapevine-growing season extends from October to March, while the dormancy season spans from May to September (Jones, 2012). The dataset analyzed in this study included two growing seasons (2022–2023 and 2023–2024) and the 2023 dormancy season (May to September 2023) (Table 2).

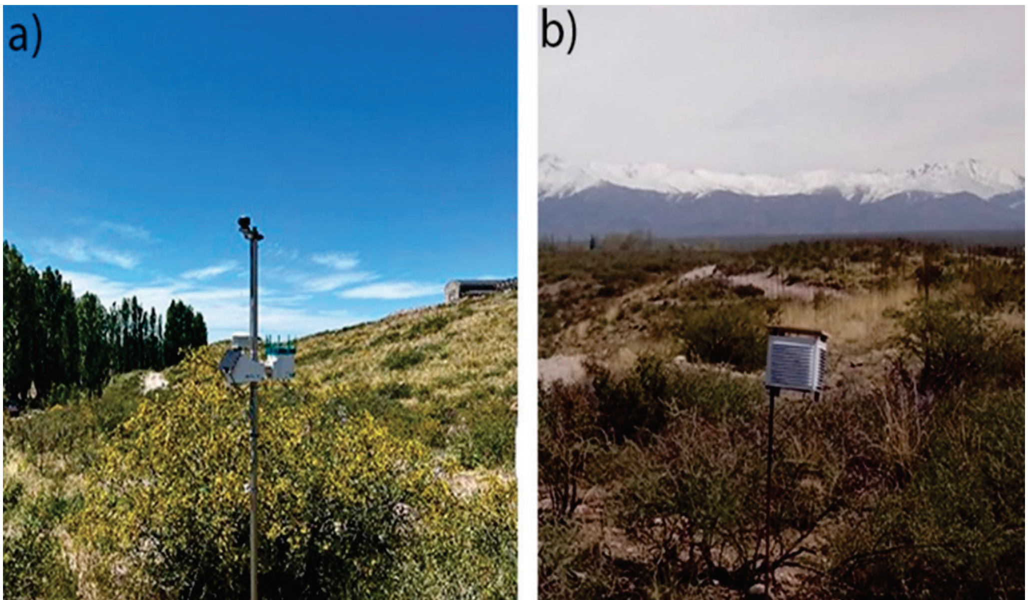

Figure 4. Instrumentation used in the study: a) μMETOS meteorological station 12A; b) HOBO Pendant MX2201 temperature sensor.

Table 1. Topographic characteristics of the locations for each temperature sensor and the 12A meteorological station.

ID Sensor	Altitude (m a.s.l)	Slope (°)	Aspect
10	1436.9	3.94	NE
11	1448	6.67	SE
12A	1450.3	7.97	E
12	1457	16.62	NE
13	1456.7	2.55	SE
14	1462.8	5.41	NE
15	1472.2	25.41	NE
16	1481	4.44	E
17	1473.1	23.71	SW
18	1463.1	7.11	NE
19	1470	24.77	NE
20	1479	15.77	E
21	1486.9	15.57	SE

Table 2. Availability of meteorological data for this study.

Sensor ID	**2022 – 2023 GS**	**2023 – 2024 GS**	**DP 2023**
10	30/10/2022 - 30/04/2023	01/10/2023 - 26/04/2024	01/05/2023 - 30/09/2023
11	30/10/2022 - 27/03/2023	01/10/2023 - 17/04/2024	01/05/2023 – 30/09/2023
12	30/10/2022 - 30/04/2023	01/10/2023 - 28/02/2024	01/05/2023 - 30/09/2023
12A		01/10/2023 - 31/03/2025	19/09/2023 -30/09/2023
13	30/10/2022 - 30/04/2023	01/10/2023 - 17/04/2024	01/05/2023 - 30/09/2023
14	30/10/2022 - 27/03/2023	01/10/2023 - 30/04/2024	12/06/2023 - 30/09/2023
15	30/10/2022 - 30/04/2023	01/10/2023 - 28/02/2024	01/05/2023 - 30/09/2023
16	30/10/2022 - 30/04/2023	01/10/2023 - 07/04/2024	01/05/2023 - 30/09/2023
17	30/10/2022 - 27/03/2023		01/05/2023 - 30/09/2023
18	30/10/2022 - 30/04/2023	01/10/2023 - 30/04/2024	15/05/2023 - 30/09/2023
19	30/10/2022 - 30/04/2023	01/10/2023 - 17/04/2024	01/05/2023 - 30/09/2023
20	30/10/2022 - 30/04/2023	01/10/2023 - 17/04/2024	01/05/2023 - 30/09/2023
21	30/10/2022 - 30/04/2023	01/10/2023 - 30/04/2024	01/05/2023 - 30/09/2023

3. Methods

The section describes the meteorological variables, bioclimatic indices, and statistical methods used to analyses microclimatic variability in the Monasterio vineyard. Data from the 12A weather station were used to characterize diurnal cycles of meteorological variables during the growing season.

Quality control procedures were applied to identify inconsistencies and potential sensor malfunctions. A systematic daytime warm bias was detected in several sensors, likely associated with limited ventilation in passive radiation shields. To correct this bias, hourly correction factors were calculated based on the mean temperature difference between Sensor 12 and a reference meteorological station (12A) over the period 19 September 2023–30 April 2024. Corrected temperature values was obtained as (Eq. 1):

$$\mathrm{T_{corr}(i) = T_{raw}(i) - \Delta_{12-12A}}(h) \quad \text{(Eq. 1)}$$

Where Δ_{12-12A} represents the mean hourly bias. These correction factors were subsequently applied to all sensors, reducing systematic errors while preserving spatial temperature variability. Since all HOBO sensors were of the same model and deployed under similar conditions, a consistent bias across the network was assumed.

Heat and cold accumulations were analysed for the October 2023–March 2024 growing season using bioclimatic indices recommended by the International Organization of Vine and Wine (OIV, 2015; Table 3), including: Absolute minimum temperature of the year ($\mathrm{Tmin_{abs}}$), Chill hours (CH), Winkler Index (WI), Night Coolness Index (CI).

Potential solar radiation was estimated for the growing season (October–March) using the *r.sun.insoltime* tool in GRASS GIS within QGIS software, under clear sky conditions and considering topographic shading effects of the Andes. Calculations were based on topographic variables (elevation, slope, and aspect) derived from a 1 m resolution Digital Elevation Model (DEM) provided by the RAQUIS project.

Table 3. Bioclimatic indices recommended by the OIV technical specifications (2012) calculated for the 2023–2024 growing season.

Bioclimatic Indices	Equation	Classification
Absolute minimum temperature of the year ($\mathrm{Tmin_{abs}}$). Castillo and Castellví Santos (2001) Hall and Sadras (2009)	$\mathrm{LMT}=\frac{1}{\mathrm{N}}\sum_{1}^{\mathrm{N}}\mathrm{Tmin_{abs}}$ Being N the number of years considered in the study, and $\mathrm{Tmin_{abs}}$ the absolute minimum temperature recorded for each year.	The occurrence of minimum temperatures below -15°C and -20 °C can be hazardous for grapevines.
Chilling hours (CH) Horvath *et al.* (2003) Londo and Kovaleski (2019)	$\mathrm{CH}=\sum_{\mathrm{May,1st}}^{\mathrm{September,30}}\mathrm{Hours_{0°C<Tmean_h<7.2°C}}$ Being $\mathrm{Hours_{0°C<Tmean_h<7.2°C}}$ the summation of hours in dormancy when hourly mean temperatures ($\mathrm{Tmean_h}$) was between 0 and 7.2 °C.	Vitis Vinifera cultivars typically require 50–400 chilling hours
Winkler Index (WI) Amerine and Winkler (1944) OIV (2012) Massano *et al.* (2023)	$\mathrm{WI}=\sum_{\mathrm{April,30}}^{\mathrm{October,1st}}(\mathrm{Tmean_d}-10)$ where, $\mathrm{Tmean_d}$ is the daily mean temperature. Only days with a Tmean > 10°C are considered.	- Very cold (<850 GD) - Region 1 (850-1389 GD): cold climates. - Region 2 (1390-1667 GD): moderately temperate climate. - Region 3 (1668- 1944DD): warm climates. - Region 4 (1945 – 2222 DD): hot climates. - Region 5 (2223 – 2700 DD): very hot climates - Too hot (>2700 DD)
Night Coolness Index (CI) Tonietto and Carbonneau (2004) OIV (2012) Massano *et al.* (2023)	$\mathrm{CI}=\frac{1}{\mathrm{N}}\sum_{\mathrm{March,1st}}^{\mathrm{March,31}}\frac{\mathrm{Tmin_d}}{31}$ where, $\mathrm{Tmin_d}$ is the daily minimum temperature recorded during the month of March.	- (CI+2) = very cold night CI ≤ 12°C. - (CI+1) = cold nights 12°C <CI≤14°C. - (CI-1) = template night. 14°C <CI≤18°C. - (CI-2) = warm nights 18°C >CI.

To analyze spatial thermal variability, multiple linear regression model developed using the Regression Analysis tool in SAGA QGIS (Bostan *et al.,* 2012; García and Díaz, 2023; Mansourmoghaddam *et al.,* 2024; Raillani *et al.* 2022). Topographic variables (elevation, slope, and aspect derived from the digital elevation model) were used as predictor, while thermal (Tmin, Tmax, Tmean, ΔT), and bioclimatic indices (CH, WI, and CI) were derived from in situ observations. The regression models were applied to the corresponding topographic raster layers to generate continuous spatial distributions at the same resolution. This approach allows the estimation of temperature patterns based on terrain–climate rather than distance-based interpolation. Model performance was evaluated using a leave-one-out cross-validation (LOOCV) approach, in which individual observations were iteratively excluded from model calibration. Predictive accuracy was quantified using root mean square error (RMSE) and mean absolute error (MAE). Residuals were further analyzed and interpolated using a multilevel B-spline method to capture local variability not explained by the regression models. Nearest-neighbor resampling was used only to ensure spatial alignment between raster datasets

After obtain the continuous spatial maps of the meteorological variables and bioclimatic indices, a multiple linear regression model (Eq. 2) was constructed, and the relative weights of each variable were calculated as the proportion of the absolute value of its coefficient to the total sum of absolute coefficients (Eq. 3), as follows:

$$y = a * \text{altitude} + b * \text{slope} + c * \text{aspect} \qquad \text{(Eq. 2)}$$

Where altitude, slope, and, aspect[1] are the independent or predictor variables; y is the thermal dependent or predicted variable; and a, b, and c are the regression coefficients of the multiple linear regression model.

$$W_a = \frac{a}{a+b+c} * 100\%,\ W_b = \frac{b}{a+b+c} * 100\%, \text{ and } W_c = \frac{c}{a+b+c} * 100\% \qquad \text{(Eq. 3)}$$

WhereW_a, W_b and, W_c are the relative weights of each independent (topographic) variable.

Thermal risk was assessed using GIS-based mapping and binary classification criteria. For cold risk, a value of 1 was assigned when any of the following conditions were met:

(i) High accumulation of chilling hours, increasing vulnerability to late frost (High chilling hour accumulation reduces heat requirements and advances phenological development, thereby increasing exposure and vulnerability to late spring frost (Hu *et al.,* 2022; Chu *et al*., 2023);

(ii) Minimum temperatures during dormancy approaching −15 °C (Table S3);

(iii) Temperatures below 0 °C during the growing season (Castillo and Castellví Santos, 2001).

The sum of these criteria was used to classify risk into three levels (1 = low, 2 = medium, 3 = high).

High-temperature risk was evaluated using three criteria (Jones, 2012):

(i) Tmax > 35 °C;

(ii) Tmax > 40 °C;

(iii) Mean growing-season temperature > 21 °C.

These criteria were combined to define low, medium, and high risk levels.

[1] In this case aspect was reclassified into 16 directional sectors (22.5° intervals). Each sector was assigned its corresponding central angle (e.g., 0°, 22.5°, 45°, etc.). Although aspect is inherently a circular variable, this discretisation provides a practical approximation of directional effects at the spatial scale of the study, allowing its integration within the linear modelling framework.

A composite thermal risk map was generated by summing cold and heat risk values, resulting in scores ranging from 2 to 6. These values were reclassified into five risk levels: very low (2), low (3), medium (4), high (5), and very high (6).

4. Results

This section presents the results derived from meteorological measurements within the vineyard, focused on the characterization of its local microclimate.

4.1. Mean Diurnal cycles of meteorological variables during the 2023-2024 growing season

A comparison between Sensor 12 and the reference station (12A) revealed a systematic temperature bias. After applying hourly correction factors, this bias was substantially reduced, and the corrected series showed strong agreement with the reference data, with mean hourly errors close to zero. The correction was applied to all sensors to ensure comparability and minimise systematic bias.

Figure 5 shows the hourly mean of incoming solar radiation, wind, and temperature during the 2023–2024 growing season. Solar radiation, measured at the 12A, followed a clear diurnal cycle, beginning around 07 Local Time (LT) and extending until approximately 21 LT, resulting in a daylight period of about 14 hours (Fig. 5a). Maximum radiation values were observed between 13 LT and 14 LT, close to the local solar noon (Argentina Time Zone (UTC-3)). Recall that this hourly distribution represents a seasonal average for the growing period, when days are longest and solar irradiance is most intense (Fig. 5a). Low but non-zero radiation values persisted after 19 LT, reflecting the shading effect of the Andes Mountain range.

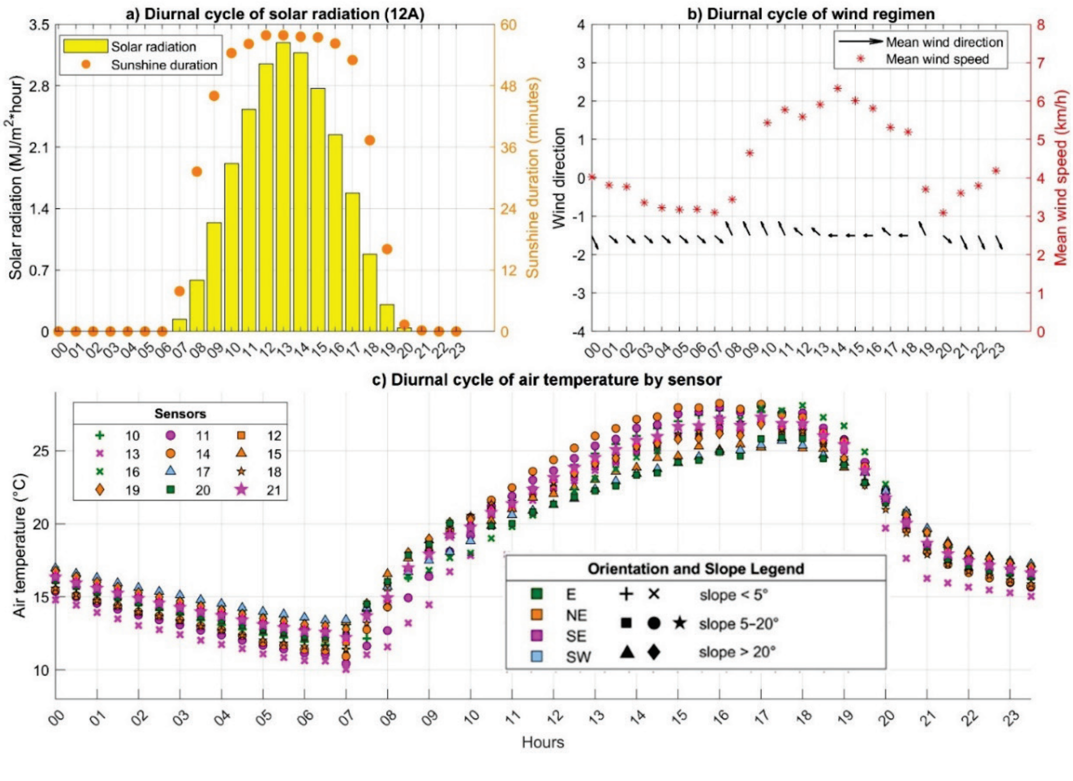

Figure 5. Hourly mean of: a) incident solar radiation per hour (MJ m^{-2} h^{-1}), b) wind intensity and direction, and c) temperature of different sensors for the 2022–2023 and 2023–2024 growing seasons. Different symbols and colors represent different orientation and inclination of the surrounding terrain. Time is expressed in Local Time (UTC-3).

The mean diurnal cycle of wind speed showed a thermally driven regime, consistent with mountain–plain circulation patterns (Fig. 5b). Wind speeds increased during daytime and decreased at night, indicating the development of upslope and downslope flows associated with diurnal heating and cooling cycles (Whiteman, 2000). This pattern was consistent with typical summer conditions in the Andean piedmont.

Mean air temperature, calculated at 30-minute intervals across the growing season, exhibited marked spatial differences in the diurnal cycle (Fig. 5c). The dominant pattern was controlled by daytime radiative heating and nocturnal cooling. Night-time temperature decreases were relatively uniform across sensors; with parallel cooling rates and minimum temperatures occurring almost simultaneously between 06:30 and 07:00 LT. Despite this temporal coherence, substantial differences in the minimum temperature were observed, reaching up to 3.5 °C between sensors. The lowest values (10-11.5 °C) were recorded at sensors 11, 13, 14, and 18, located in lower terrain positions (Fig. 2a, Table 2), whereas highest minimum temperatures (11.5-13.5°C) were observed at sensors 15, 16, 17, 19, and 21, situated at higher elevations or on steeper slopes (Fig. 2a and 2b).

The timing of maximum temperatures showed greater variability among sites (Fig. 5c). Maximum temperatures occurred around 16:00 LT at sensors 10, 11, 13, and 14; between 17:00–17:30 LT at sensors 12, 17, 18, 19, 20, and 21; and around 18:00 LT at sensors 15 and 16. In contrast, the magnitude of maximum temperatures showed limited spatial variations, ranging from approximately 26°C (sensor 17) to slightly above 28°C (sensor 14). After sunset behind the Andes (around 19 LT), air temperature decreased rapidly across all sites. The variability in the timing of maximum temperature suggests differences in local energy balance and near-surface air mixing across the vineyard.

4.2. Spatial variability of the local temperatures and cold and heat accumulation.

Ridgeline plots of kernel density estimates at each sensor site are shown in Figure 6 and illustrate intra-vineyard thermal variability. Tmin distributions were narrowly concentrated between 10°C and 15°C, with probability density decreasing rapidly toward higher values and more gradually toward lower values (Fig. 6a). Sensors 10, 11, 13, 14, and 18 showed distributions toward lower temperatures, whereas sensors 16, 17, and 19 were shifted toward higher temperatures.

Tmax distributions (Fig. 6b) showed a broader spread compared to Tmin (Fig. 6a). Sensor 16 exhibited the widest distribution, with higher probability density extending toward higher temperatures. Sensors 12, 15, 17, and 20 showed Tmax distributions shifted toward lower values, generally below 30°C, whereas sensors 11, 14, 18, 19, and 21 showed distributions shifted toward higher values, with peaks slightly above 30 °C. Secondary peaks above 40°C were observed at sensors 16, 18, and 20.

The ΔT distributions were mainly concentrated between 10°C and 25°C (Fig. 6c). Higher amplitudes, with peak densities near 25°C, were observed at sensors 10, 11, 13, and 14, located in the central sector of the vineyard. Lower amplitudes, with peaks around 17°C, were observed at sensors 12, 17, and 20.

Heat accumulation during the 2023–2024 growing season were analysed using cumulative thermal indices, excluding sensors 12, 15, and 17 due to missing data in March 2024. The Winkler Index revealed two distinct viticulture climate classes (Fig. 7a). Most sensors were classified as Region II (temperate), whereas sensors 16 and 19 were classified as Region III (warm). Sensors 10, 11, 14, and 21 were located near the boundary between both regions. Sensor sites experiencing strong afternoon heating (10, 11, 14, and 21) remain close to the Region III boundary. Sensor 16, located on the hilltop, shows strong afternoon heating, and both sites 16 and 19 exhibit the mildest morning cooling. In fact, site 19 also has one of the lowest diurnal thermal amplitudes.

Cold accumulation was analyzed using CI and CH. The Night Coldness Index (CI), used to evaluate grape ripening, is shown in Figure 7b. The CI indicates a single predominant thermal category across all sensor sites: very cold nights. During the dormancy season (May to September), the accumulation of CH approximately 1700 hours across all available sensors (Fig. 7c). Higher values of chilling hours (~2000 hours) were recorded by sensors 10, 11, and 13, all located in areas with gentle slopes (<7°) in the middle of the vineyard, followed by sensors 18, 20, and 21 along a valley to the south of the hill (Fig. 3a-b). Sensors 10, 11, 14, and 18 recorded absolute minimum temperatures around –10 °C (Fig. 7c), while sensor 13 registered an absolute Tmin near –14 °C, indicating a cold-air pooling effect in a topographic depression, also evident for extreme Tmin.

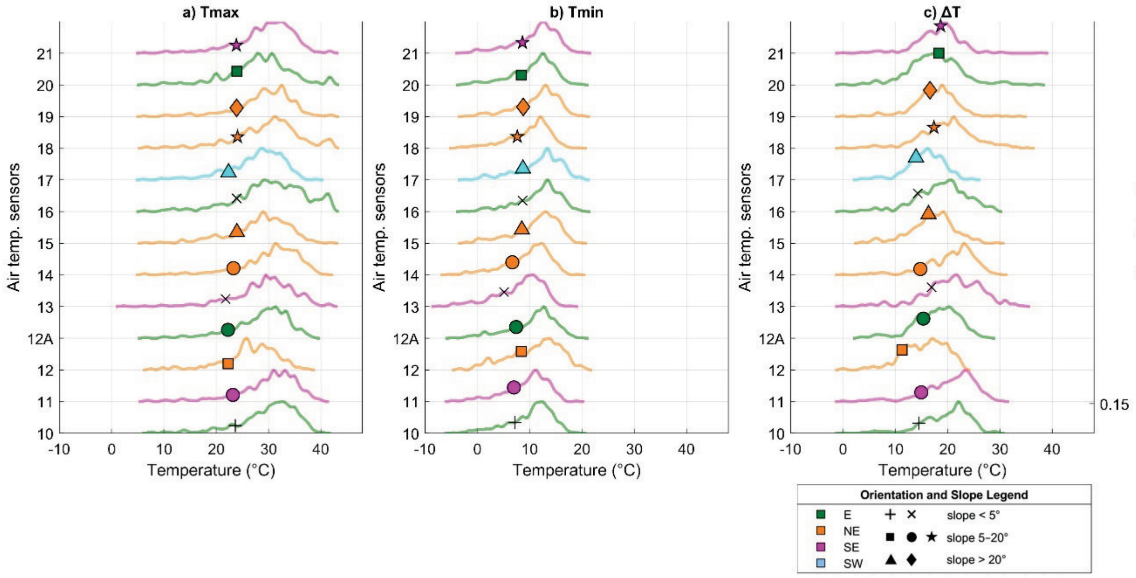

Figure 6. Ridgeline plots for a) Tmin, b) Tmax, and c) ΔT at each sensor site for the 2022–2023 and 2023-2024 growing seasons. The different color lines and markers indicate different orientation and slope of the laying terrain on each sensor. The limits of y axis with the probability density are 0 and 0.15 for all the plots.

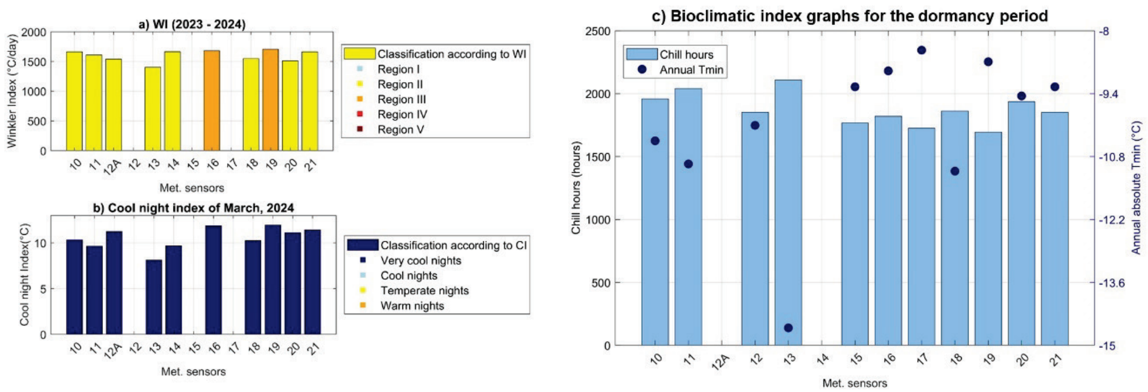

Figure 7. Bioclimatic indices for the 2023–2024 growing season: a) Winkler Index, b) Night Coldness Index, c) the accumulated chilling hours between May and September 2023 and the absolute minimum temperatures.

The map of modelling solar radiation during the growing season (Fig. 8a) reveal large spatial differences across the vineyard. Lowest radiation values were observed on south-facing slopes of the central hill, around sensor 17 (Fig. 3c), while the highest incidence is observed in areas with gentle slopes facing N, NE, and E, corresponding to sensors 10, 11, 12A, 14, 16, 18, and 21. Terrain oriented in the northeast quadrant, but with slightly steeper slopes, receives moderate solar radiation, such as the north-facing side of the hills.

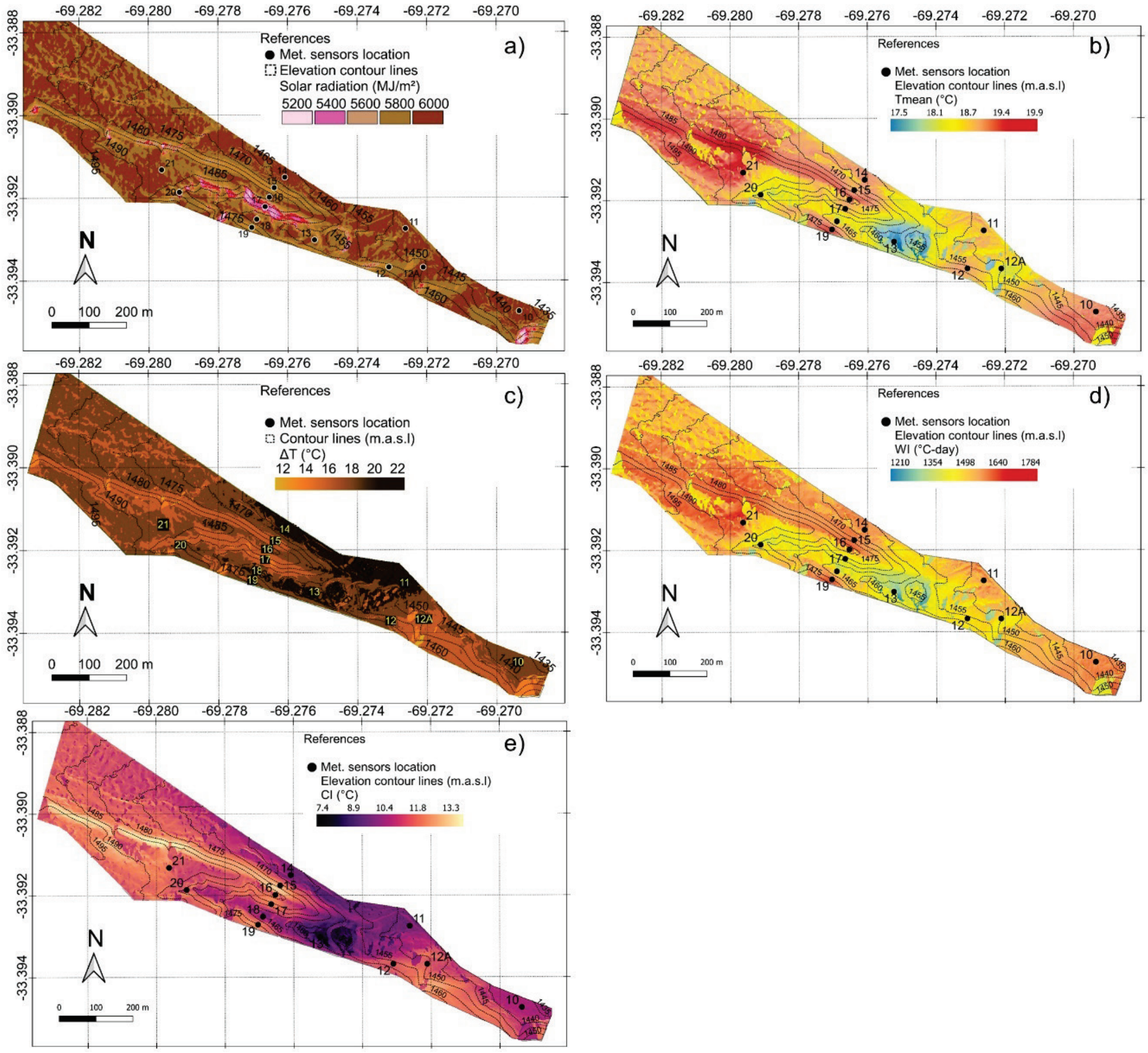

Figure 8. Spatial distribution of potential cumulative solar radiation during the whole growing season within the vineyard, temperature variables and interpolated bioclimatic indices across the vineyard during the growing season: a) potential cumulative solar radiation, b) mean temperature, c) diurnal temperature range, d) Winkler Index, e) Night Coolness Index.

To generate continuous maps of meteorological variables (Tmin, Tmax, Tmean, and ΔT) and bioclimatic indices (CH, WI, and CI), model performance was evaluated using a leave-one-out cross-validation (LOOCV) approach. The results of the Regression Analysis tool (SAGA QGIS) indicate a good agreement between observed and predicted values. For temperature variables, RMSE values ranged from 0.33°C (Tmean) to 0.99°C (ΔT), with mean absolute errors below 0.7°C. These errors represent approximately 8-11% of the observed variability for Tmax, Tmin, and ΔT, and around 11% for Tmean. Bioclimatic indices showed higher absolute errors (RMSE ≈ 61 for WI and CH, and 0.50°C for CI); however, these correspond to approximately 6–10% of their observed ranges, reflecting the cumulative nature of these indices. Overall, the model provides a reasonable representation of spatial thermal variability across the vineyard, supporting the use of the derived continuous surfaces to analyze topoclimatic patterns and identify zones of differential thermal behavior.

The spatial variability in solar radiation (Fig. 8a) drives marked differences in thermal variables and indices across the vineyard (Fig. 8b–e). Across the study area, Tmean ranges from 17 to 20°C with an altitudinal gradient of approximately 0.1°C per 10 m. Higher Tmean values were observed in the lower sector of the vineyard, surrounding sensor 10, on the northeast-facing slopes of the central and southern hills around sensors 15 and 19, and in the higher sector of the vineyard near sensors 20 and 21

(Fig. 8b). Lower Tmean values are observed in the depression used as a water reservoir around sensor 13, at the valley bottom between the central and southern hills, and on the south-facing slopes of the central hill. Areas with lower Tmean generally correspond to zones of reduced solar radiation (Fig. 8a). However, higher Tmean values do not always coincide with maximum radiation input, suggesting that turbulent mixing plays a key role in redistributing heat within the vineyard. The ΔT ranged between 12°C and 22°C (Fig. 8c), with a negative altitudinal gradient of −0.2°C per 10 m. The highest ΔT values are found in the middle sector of the vineyard, consistent with the patterns inferred from the sensor network.

The Winkler Index ranged from 1,207 to 1,790°C·day and showed spatial patterns consistent with Tmean (Fig. 8d). Higher values are observed in both the upper and lower sectors of the vineyard, as well as in the central-northern area, particularly on the north-facing slope of the central hill. The CI ranges from 7 to 15°C, with an altitudinal gradient of 0.28°C per 10 m. Lower CI values are concentrated in the trough and at the valley bottom, highlighting zones of enhanced nocturnal cooling. These areas are particularly relevant for grape ripening, as CI is a key indicator of night-time thermal conditions (Fig. 8e).

4.3. Linear Regression model and heatmaps

A multiple linear regression analysis was conducted to explore the influence of topographic variables (altitude, slope, and aspect) on the spatial distribution of thermal variables and bioclimatic indices (solar radiation, Tmax, Tmin, Tmean, ΔT, WI, CH, and CI). Relative contributions of predictor variables were derived from regression coefficients (Eqs. 2–3) to identify the dominant controls on each variable (Table 4).

Table 4 show that solar radiation, Tmax, and ΔT were most strongly correlated with slope and aspect, while Tmin, CH, and CI were primarily correlated with altitude and slope. Tmean and WI showed their strongest associations with altitude and aspect. The spatial patterns derived from the regression models are shown in Figure 9. Model results indicated higher potential solar radiation on slopes oriented toward the NE, E, and SE, particularly for gentle slopes (5°–20°; Fig. 8a). Lower radiation values were associated with slopes oriented toward the SW, W, and NW, with moderate inclinations of 20°–30°, receiving about 15%–25% less than the maximum solar radiation value (5834 MJ m^{-2}).

Table 4. Relative contributions of altitude, slope, and aspect to the variability of meteorological and bioclimatic indices based upon the interpolated, gridded data. Values in red and italics indicate the highest relative weights recorded for each dependent variable.

Met. Variable	Altitude	Slope	Aspect
Solar radiation	4.06	*35.50*	*60.44*
Tmax	12.82	*27.91*	*59.27*
Tmin	*53.75*	*37.08*	9.17
Tmean	*26.72*	1.10	*72.18*
ΔT	12.21	*40.50*	*47.29*
WI	*18.88*	9.62	*71.50*
CH	*27.06*	*62.07*	10.87
CI	*46.72*	*33.43*	19.85

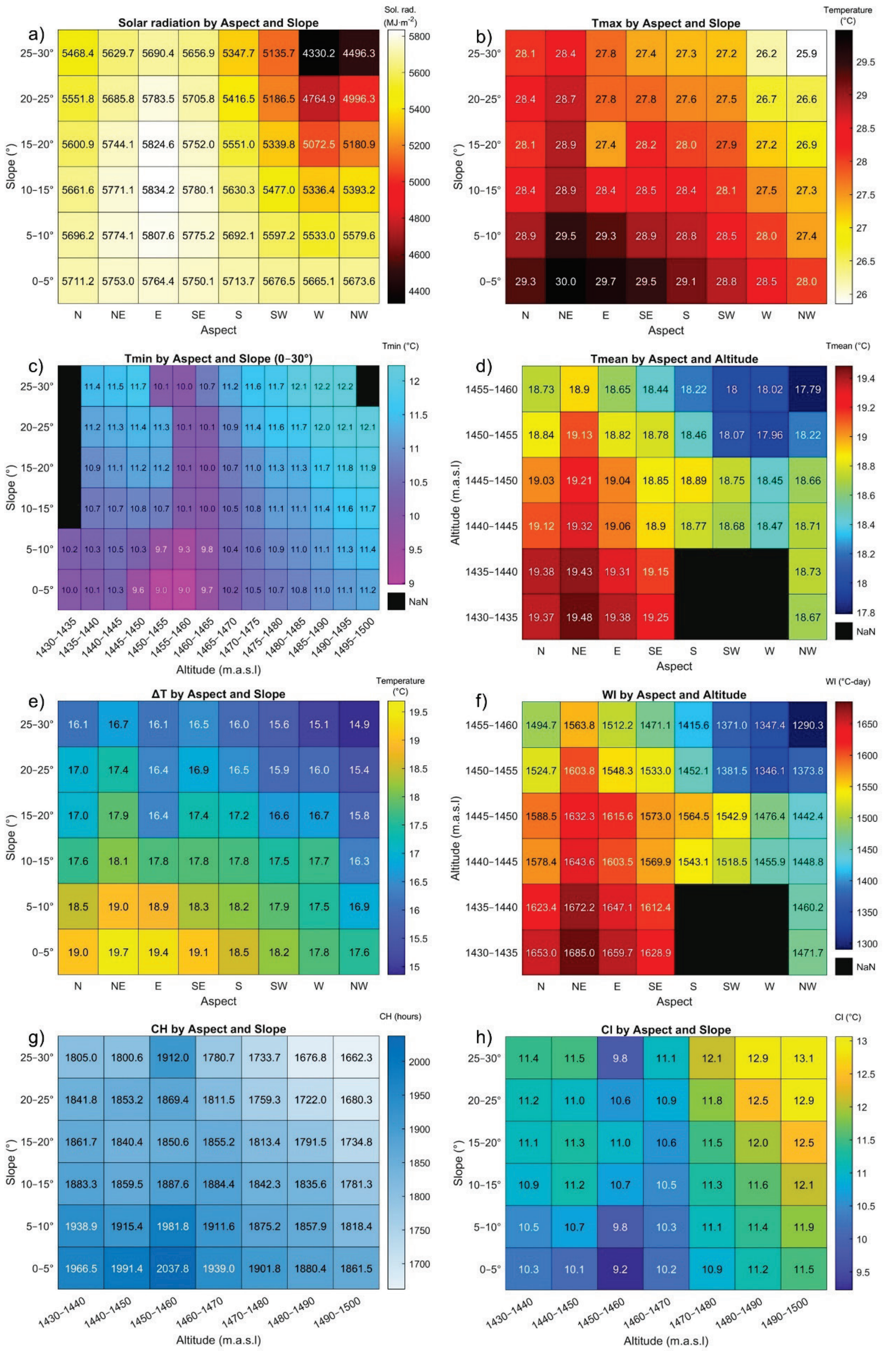

Figure 9. Heatmaps with results of linear multiple regression model predicting solar radiation, thermal variables and bioclimatic indices during the 2023-2024 growing season according to topographic characteristics of the terrain: a) Potential Solar cumulative radiation, b) Tmax, c) Tmin, d) Tmean, e) ΔT, f) Winkler index, g) night coolness index, h) chilling hours during the dormancy period.

For Tmax (Fig. 9b), the highest values were associated with NE- to SE-facing slopes and low slopes angles (<10°), closely following the input of solar energy. In particular, terrain facing NE remained warmer regardless of slope. Lower Tmax values were observed on W- and NW-facing slopes. Tmin (Fig. 9c), which showed stronger dependence on altitude and slope (Table 4), showed its lowest values at mid-level altitudes within the vineyard, especially on slopes below 5°.

For Tmean (Fig. 9d), higher values at lower altitudes over NE-oriented slopes, while lowest values occurred at higher altitudes over W-oriented slopes. The difference between the warmest and coldest Tmean zones exceeded 1 °C. Similar to the hottest sector of Tmax, the highest ΔT values were observed on NE-oriented and flatter terrain, while the lowest ΔT values were visualized on W- and NW-oriented, steeper terrain with the lowest solar radiation (Fig. 9e).

For heat accumulation (Fig. 9f), the highest WI values were found on slopes facing the NE quadrant and at lower elevations, whereas the lowest WI values were found on slopes facing the SW and NW quadrants and at higher elevations, consistent with the spatial pattern of Tmean (Fig. 8d). Regarding cold accumulation (Fig. 9g–h), both indices (CH and CI) showed lower values at mid-elevations and on flatter terrain within the vineyard, closely matching the Tmin–topography relationship (Fig. 9c).

4.4. Risk Maps Associated with the Thermal Stress

This section analyses spatial patterns of thermal risk, identifying areas prone to extreme low and high temperatures and delineating zones of potential thermal stress. The risk maps are shown in Figure 10.

High risk of low temperatures was identified in areas surrounding sensors 11 and 14, located near the northern boundary of the central sector, and around sensors 13 and 18, associated with low-elevation terrain such as valley bottoms and the water reservoir (Fig. 10a). In contrast, lower risk levels were observed near station 12A and sensors 15, 17, 19, and 21. High-temperature risk was more limited in spatial extent and was mainly concentrated near sensor 10, located in the lowest and flattest sector of the vineyard (Fig. 10b). Most of the vineyard was classified as medium risk, except for areas around sensors 12, 17, and 20, which were classified as low risk. The area exposed to low-temperature risk (2.8 ha) was larger than that exposed to high-temperature risk (0.2 ha).

The combined thermal risk map (Fig. 10c) indicated that the highest vulnerability was concentrated around sensors 10, 11, 13, 14, and 18, covering approximately 2.6 ha (~10% of the vineyard). Areas of low to very low risk were located near sensors 12, 15, 17, 19, and 20, covering 16.8 ha (~57%). The remaining area (10.3 ha; ~33%) was classified as medium risk. No areas were classified as very high risk. Within areas classified as low to very low risk (Fig. 10c), elevations between 1,461 m and 1,490 m represented approximately 68% of the surface. Slopes between 5° and 25° accounted for more than 90% of these areas. Northeast-facing slopes covered 41% of the area, followed by north-facing (18.7%) and southeast-facing slopes (10%) (Fig. 10d).

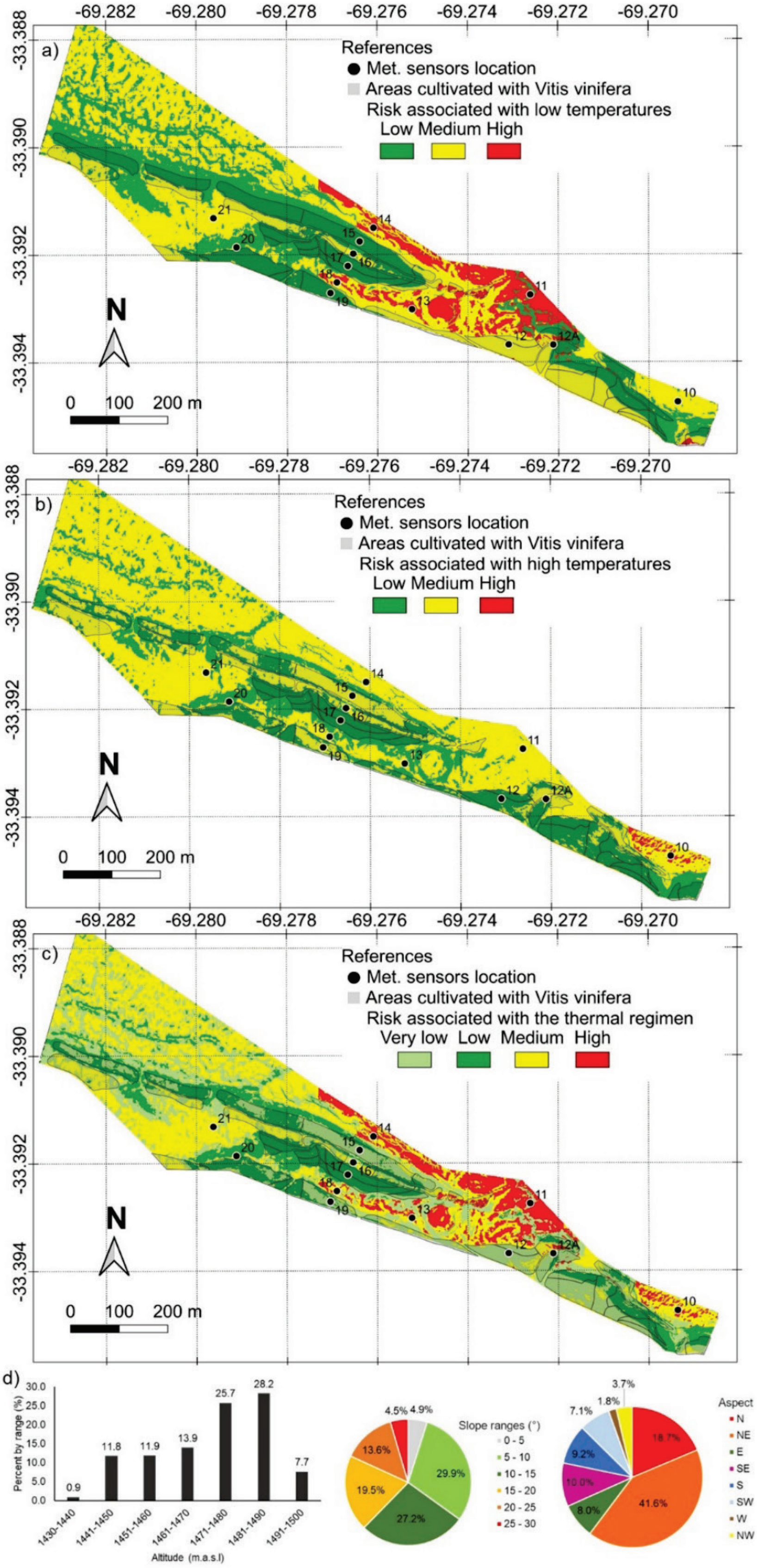

Figure 10. Thermal risk maps for: a) low temperatures, b) high temperatures, c) combination of both, d) distribution of topographic characteristics of the specific area of vineyard with very low and low temperature risk.

5. Discussion

The results of this study indicate that local topography plays a major role in shaping thermal patterns within the RAQUIS Monasterio vineyard, generating a heterogeneous microclimate at the intra-vineyard scale. The WI revealed the coexistence of two distinct viticulture climate regions (Regions II and III) within a relatively small area, highlighting the magnitude of fine-scale thermal variability. Although the influence of topography on thermal behaviour has been widely documented, e.g., Saint-Émilion (De Rességuier *et al.,* 2016), the Douro Valley (Jones and Alves, 2012), Stellenbosch (Bonnardot *et al.,* 2012), Canelones (Uruguay) (Fourment *et al.,* 2017), most studies have focused on regional or meso-scale variability. In contrast, the present study provides high-resolution insights into local climate variability, showing that significant thermal contrasts can occur over short distances within a single vineyard.

Fine-scale thermal variability arises from the interaction between regional atmospheric circulation and local terrain, as well as from the continuous exchange of heat between the land surface and the near-surface atmosphere. At the regional scale, the eastern Andean piedmont is characterised by the dominance of continental air masses during the growing season due to the orographic barrier of the Andes. This results in high solar radiation, low atmospheric humidity, and a pronounced diurnal thermal amplitude (Servicio Meteorológico Nacional, 2024). Periodic intrusions of moist air may trigger convective storms (Benedicto *et al.,* 2025; Viale and Garreaud, 2014), introducing additional variability. Observations from the vineyard (Fig. 2 and 5a) are consistent with these regional characteristics, which provide the boundary conditions for the development of local microclimates.

At the local scale, thermally driven mountain–piedmont circulations contribute to spatial temperature differences. During daytime, the observed dispersion in temperature and the variability in the timing of maximum temperatures (Fig. 5c) suggest the influence of enhanced mixing processes associated with differential solar heating across slopes (Whiteman, 2000). In contrast, nocturnal conditions are characterised by more stable and stratified near-surface air (Fig. 5c). The parallel cooling rates and the near-synchronous occurrence of minimum temperatures across sensors indicate a well-organised thermal regime. These patterns are consistent with cold-air drainage and accumulation in topographic depressions, as described in previous studies of complex terrain (Bonnardot and Cautenet, 2009; Neethling *et al.,* 2019).

The multiple linear regression model (Table 4) provides a first-order approximation of the relationships between topographic variables and thermal patterns. The results suggest that minimum temperature and cold-related indices are more strongly associated with elevation and slope, whereas maximum temperature and heat-related indices show stronger relationships with slope and aspect. Although non-linear relationships may exist, the linear approach allows a transparent and interpretable assessment of the relative contribution of each predictor. This is particularly relevant for site-specific management, where model interpretability is often prioritised. More complex approaches may capture additional interactions, but the linear framework provides a useful baseline for analysing topoclimatic variability.

Differences in slope, aspect, and altitude create marked contrasts in solar energy input (Fig. 9a), leading to substantial variability in Tmax and its timing (Fig. 5c). North- and east-facing slopes with gentle inclines exhibit the highest and earliest Tmax values (Fig. 9b). The crest area, influenced by air mixing between opposing slopes, does not exhibit the extremes of either Tmax or Tmin but registers high mean temperatures and Winkler index values (Fig. 8d), illustrating the complex interplay between topography and airflow on heat accumulation. The west-facing slopes receive up to 25% less solar radiation than east-facing slopes due to the pronounced shading effect of the high Andes at sunset. This quantifies the rapid decline in sunshine observed after 18:00–19:00 LT by the weather station, highlighting how terrain-induced shading modulates microclimatic variability.

The thermal risk maps translate directly into management zones for precision viticulture in Monasterio. Since cold-related risk (Fig. 10a) outweighs heat risk (Fig. 10b), frost prevention should be prioritized in operational planning. Low-temperature hotspots -particularly depressions and valley sectors near sensors 11, 14, and 18- are designated as 'critical frost units'. In these zones, vineyard design should focus on reducing cold-air residence time and protecting sensitive phenological stages. Recommendations include prioritizing frost-tolerant or late-budding cultivars, employing higher training systems, and adopting delayed or double pruning to bypass peak frost windows. These sectors are also primary candidates for active protection (e.g., wind machines or heaters), supported by dense monitoring to trigger interventions. Conversely, low-risk zones (Fig. 10c) -typically at intermediate elevations (1461–1,90 m a.s.l.) on moderate slopes (5°–25°) with NE, N, and SE aspects- are the most suitable for new plantings of frost-sensitive varieties, as they balance heat accumulation with reduced cold-air pooling. Medium-risk areas should function as transition units, where passive measures like optimized row orientation and unobstructed cold-air drainage pathways are prioritized.

A limitation of this study is the temporal coverage of the dataset. While temperature variables (Tmean, Tmin, Tmax, and ΔT) were analysed over two growing seasons and one dormancy period, bioclimatic indices were derived from a single complete growing season due to data gaps. This may limit the representation of interannual variability. However, the primary objective of this study was to characterise spatial patterns of thermal variability driven by topography. As these patterns are largely controlled by terrain attributes, they are likely to be more stable over time than temporal variability. Therefore, the identified spatial contrasts are considered representative of the local topoclimatic structure.

Under future warming conditions, fine-scale topographic variability may play an important role in modulating local climate within vineyards. While regional temperatures are expected to increase, local microclimatic differences may help maintain suitable conditions in specific areas. This highlights the importance of site-specific management for climate adaptation in mountain viticulture. Overall, this study demonstrates the value of integrating high-resolution temperature monitoring with terrain analysis to characterise intra-vineyard thermal variability and support decision-making in precision viticulture.

6. Conclusions

This study demonstrates that local topography plays a major role in shaping thermal variability within the RAQUIS Monasterio vineyard, generating marked microclimatic contrasts at the intra-vineyard scale. Differences in elevation, slope, and aspect control solar radiation and temperature patterns, leading to distinct thermal zones over short distances. The results highlight the importance of fine-scale topographic variability in determining both heat accumulation and frost occurrence. In particular, low-lying areas and topographic depressions were identified as zones prone to cold-air accumulation, revealing that frost represents a major climatic risk within the vineyard. This finding shows that local topoclimatic conditions can significantly influence exposure to thermal extremes, even within a relatively small area.

From a practical perspective, this approach provides a framework for identifying whether a given area is more sensitive to cold, heat, or a combination of both. This information is essential for precision agriculture, as it supports the delineation of thermal zones for site selection, variety allocation, and management practices. In this context, low-lying sectors may require frost mitigation strategies, whereas warmer areas may benefit from adjustments in canopy and water management to reduce heat stress.

The methodological approach, based on the integration of dense temperature monitoring and GIS-based spatial modelling, provides a transferable framework for analysing microclimatic variability in complex terrain. This approach can be applied in other mountainous or undulating regions, offering a practical tool for identifying spatial patterns of thermal risk and supporting site-specific management strategies.

Overall, this study highlights the value of high-resolution microclimatic analysis for understanding terrain–atmosphere interactions and supporting adaptive management in agricultural systems. Future research incorporating longer time series would allow a more comprehensive assessment of interannual variability and extreme events. In addition, further work will place particular emphasis on the characterisation of frost events, given their relevance as a key climatic risk, and on refining local-scale assessments of thermal variability in complex terrain. Non-linear modelling approaches may also be explored to better capture complex interactions between topography and temperature.

Acknowledgments

The authors gratefully acknowledge the Consejo Nacional de Investigaciones Científicas y Técnicas (CONICET) for supporting this research through a postdoctoral fellowship under which the present work was conducted. Appreciation is also extended to the RAQUIS project for supporting the research, data, and logistical assistance. Special thanks to Dr. Diego C. Araneo for his valuable support in statistical analysis. The authors would also like to thank the Editorial Committee of Cuadernos de Investigación Geográfica for their valuable work, as well as the anonymous reviewers for their constructive comments and suggestions, which have significantly improved the quality of this manuscript.

References

Amerine, M.A., Winkler, A.J. 1944. Composition and quality of musts and wines of California grapes. *A Journal of Agricultural Science*. Published by the California Agricultural Experiment Station 15, 493-673.

Benedicto, M., Viale, M., Salio, P. 2025. Summer convection over and around the subtropical Andes. *Quarterly Journal of the Royal Meteorological Society,* e4992. http://doi.org/10.1002/qj.4992

Bonnardot, V., Cautenet, S., 2009. Mesoscale modeling of a complex coastal terrain in the South Western Cape using a high horizontal grid resolution for viticultural applications. *Journal of Applied Meteorology and Climatology* 48, 330-348. http://doi.org/10.1175/2008JAMC1710.1

Bonnardot, V., Carey, V., Madelin, M., Cautenet, S., Coetzee, Z., Quénol, H. 2012. Spatial variability of night temperatures at a fine scale over the Stellenbosch wine district, South Africa. *Journal International des Sciences de la Vigne et du Vin* 46(1), 1-13.

Bonnefoy, C., Quénol, H., Bonnardot, V., Barbeau, G., Madelin, M., Planchon, O., Neethling, E. 2012. Temporal and spatial analyses of temperature in a French wine-producing area: the Loire Valley. *International Journal of Climatology* 33, 1849-1862.

Bostan, P.A., Heuvelink, G.B.M., Akyurek, S.Z. 2012. Comparison of regression and kriging techniques for mapping the average annual precipitation of Turkey. International *Journal of Applied Earth Observation and Geoinformation* 19, 115-126. https://doi.org/10.1016/j.jag.2012.04.010

Castillo, F.E., Castellví Sentis, F. 2001. *Agrometeorología*. Ediciones Mundi-Prensa, Madrid.

Chu, X., Man, R., Dang, Q.-L. 2023. Spring phenology, phenological response, and growing season length. *Frontiers in Forests and Global Change* 6, 1041369. https://doi.org/10.3389/ffgc.2023.1041369

Ciazela, M., Ciazela, J. 2021. Topoclimate mapping using Landsat ETM+ thermal data: Wolin Island, Poland. *Remote Sensing* 13, 2712. http://doi.org/10.3390/rs13142712

Daskalakis, I., Stavrakaki, M., Vardaka, K., Nikolaou, S., Koukoufiki, S., Giannakou, T., Bouza, D., Biniari, K. 2025. How altitude affects the phenolic potential of the grapes of cv. 'Fokiano' (Vitis vinifera L.) on Ikaria Island. *Environments* 12(9), 320. http://doi.org/10.3390/environments12090320

Deis, L., Martínez, L., da Costa, B.S., Vilanova, M. 2024. The influence of climatic conditions associated with altitude on the volatile composition of Cabernet Sauvignon wines from Argentina, Spain and Portugal. *Horticulturae* 10(8), 870. http://doi.org/10.3390/horticulturae10080870

De Resséquier, L., Le Roux, R., Quénol, H., Van Leeuwen, C. 2016. Spatial temperature variability and distribution at local scale in Saint-Emilion and Pomerol. En: *Climwine Sustainable Grape and Wine Production in the Context of Climate Change.* Bordeaux, France, 10-13.

Fourment, M., Ferrer, M., González-Neves, G., Barbeau, G., Bonnardot, V., Quénol, H. 2017. Tannat grape composition responses to spatial variability of temperature in Uruguay's coastal wine region. *International Journal of Biometeorology* 61, 1617-1628. http://doi.org/10.1007/s00484-017-1340-2

García, D.H., Díaz, J.A. 2023. Space–time analysis of the earth's surface temperature, surface urban heat island and urban hotspot: relationships with variation of the thermal field in Andalusia (Spain). *Urban Ecosyst* 26, 525-546. https://doi.org/10.1007/s11252-022-01321-9

Hall, A.J., Sadras, V. 2009. Whither crop physiology? En: Sadras VO, Calderini DF (Eds.), *Crop Physiology Applications for Genetic Improvement and Agronomy.* Elsevier, Amsterdam, Netherlands, pp. 545-570.

Horvath, D.P., Anderson, J.V., Chao, W.S., Foley, M.E. 2003. Knowing when to grow: signals regulating bud dormancy. *Trends in Plant Science* 8, 534-540.

Hu, Z., Wang, H., Dai, J., Ge, Q., Lin, S. 2022. Stronger spring phenological advance in future warming scenarios for temperate species with a lower chilling sensitivity. *Frontiers in Plant Science* 13, 830573. https://doi.org/10.3389/fpls.2022.830573

Irimia, L.M., Patriche, C.V., Petitjean, T., Tissot, C., Santesteban, L.G., Neethling, E., Foss, C., Le Roux, R., Quénol, H. 2024. Structural and spatial shifts in the viticulture potential of main European wine regions as an effect of climate change. *Horticulturae* 10(4), 413. http://doi.org/10.3390/horticulturae10040413

Jacquet, A., Morlat, R. 1997. Caractérisation de la variabilité climatique des terroirs viticoles en val de Loire. Influence du paysage et des facteurs physiques du milieu. *Agronomie* 17, 465-480.

Jones, G.V. 2012. Climate, grapes, and wine: Structure and suitability in a changing climate. *Acta Horticulturae* 931, 19-28. https://doi.org/10.17660/ActaHortic.2012.931.1

Jones, G.V., Alves, F. 2012. Impact of climate change on wine production: a global overview and regional assessment in the Douro Valley of Portugal. *International Journal of Global Warming* 4(3-4), 383-406. https://doi.org/10.1504/IJGW.2012.049448

Lasanta, T., Borja-Sáenz, C., Cortijo-López, M., Nadal-Romero, E., Martín, I., García-Escudero, E. 2022. Estrategias de adaptación al cambio climático en el viñedo en la cuenca mediterránea: el caso de La Rioja. *Cuadernos de Investigación Geográfica* 48, 133-156. https://doi.org/10.18172/cig.5062

Littmann, T. 2008. Topoclimate and microclimate. En: *Encyclopedia of Ecology.* http://doi.org/10.1007/978-3-540-75498-5_12

Londo, J.P., Kovaleski, A.P. 2019. Deconstructing cold hardiness: variation in supercooling ability and chilling requirements in the wild grapevine Vitis riparia. *Australian Journal of Grape and Wine Research* 25, 276-285. https://doi.org/10.1111/ajgw.12389

Mansourmoghaddam, M., Rousta, I., Ghafarian Malamiri, H., Sadeghnejad, M., Krzyszczak, J., Ferreira, C.S.S. 2024. Modelling and Estimating the Land Surface Temperature (LST) Using Remote Sensing and Machine Learning (Case Study: Yazd, Iran). *Remote Sensing* 16(3), 454. https://doi.org/10.3390/rs16030454

Massano, L., Fosser, G., Gaetani, M., Bois, B. 2023. Assessment of climate impact on grape productivity: a new application for bioclimatic indices in Italy. *Science of the Total Environment* 905, 167134. http://doi.org/10.1016/j.scitotenv.2023.167134

METOS instruments, 2025. Available at: https://metos.global/es/

Neethling, E., Barbeau, G., Coulon-Leroy, C., Quénol, H. 2019. Spatial complexity and temporal dynamics in viticulture: a review of climate-driven scales. *Agricultural and Forest Meteorology* 276-277. http://doi.org/10.1016/j.agrformet.2019.107618

Norte, F.A. 2015. Understanding and forecasting zonda wind (Andean Foehn) in Argentina: a review. *Atmospheric and Climate Sciences* 5(3), 163. http://doi.org/10.4236/acs.2015.53012

OIV. 2015. *Directrices de la OIV para estudiar la variabilidad climática en la vitivinicultura en el contexto del cambio climático* (Resolución OIV-VITI 517-2015). Available at: https://www.oiv.int/

Orlandini, S., Marta, A.D., Mancini, M. 2006. The agroclimatic analysis at farm scale. *Meteorological Applications* 13, 87-93. https://doi.org/10.1017/S1350482706002593

Prohaska, F. 1976. The climate of Argentina, Paraguay and Uruguay. En: Schwerdtfeger W (Ed.), *Climate of Central and South America.* Elsevier Scientific Publishing Company, pp. 13-112.

Raillani, B., Mezrhab, A., Amraqui, S., Amine Moussaoui, M., Mezrhab, A. 2022. Regression-based spatial GIS analysis for an accurate assessment of renewable energy potential. *Energy for Sustainable Development* 69, 118-133. https://doi.org/10.1016/j.esd.2022.06.003

Servicio Meteorológico Nacional. 2024. https://www.argentina.gob.ar/smn

Stel, L., Aranda, N.G., Haldbrandt, G., Sanchez, G. 2019. Criterios generales sobre la selección de sitios de medición, instrumental, e instalación de estaciones automáticas meteorológicas. *Nota Técnica SMN*, 2019-52.

Tonietto, J., Carbonneau, A. 2004. A multicriteria climatic classification system for grape-growing regions worldwide. *Agricultural and Forest Meteorology* 124(1-2), 81-97. http://doi.org/10.1016/j.agrformet.2003.06.001

van Leeuwen, C., Destrac-Irvine, A., Dubernet, M., Duchêne, E., Gowdy, M., Marguerit, E., Pieri, P., Parker, A., de Rességuier, L., Ollat, N. 2019. An update on the impact of climate change in viticulture and potential adaptations. *Agronomy* 9(9), 514. http://doi.org/10.3390/agronomy9090514

Viale, M., Bianchi, E., Cara, L., Ruiz, L.E., Villalba, R., Pitte, P., Masiokas, M., Rivera, J., Zalazar, L. 2019. Contrasting climates at both sides of the Andes in Argentina and Chile. *Frontiers in Environmental Science* 7, 69. http://doi.org/10.3389/fenvs.2019.00069

Viale, M., Garreaud, R. 2014. Summer precipitation events over the western slope of the subtropical Andes. *Monthly Weather Review* 142(3), 1074-1092. http://doi.org/10.1175/MWR-D-13-00259.1

Viale, M., Nuñez, M.N. 2011. Climatology of winter orographic precipitation over the subtropical central Andes and associated synoptic and regional characteristics. *Journal of Hydrometeorology* 12(4), 481-507.

Whiteman, C.D. 2000. *Mountain Meteorology: Fundamentals and Applications.* Oxford University Press, 355 pp.

Yoshino, M.M. 1975. *Climate in a small area: an introduction to local meteorology.* University of Tokyo Press, Tokio, Japón.